Desalination and Water Treatment
www.deswater.com
doi: 10.1080/19443994.2014.950994

56 (2015) 1465–1475
November

Taylor & Francis
Taylor & Francis Group

Modeling of ultrasonic cavitation as an advanced technique for water treatment

Slimane Merouani[a,b,*], Oualid Hamdaoui[a], Yacine Rezgui[c], Miloud Guemini[c]

[a]*Faculty of Engineering, Laboratory of Environmental Engineering, Department of Process Engineering, Badji Mokhtar—Annaba University, P.O. Box 12, 23000 Annaba, Algeria, Tel./Fax: +213 0 38876560; emails: s.merouani@yahoo.fr, s.merouani03@gmail.com (S. Merouani), ohamdaoui@yahoo.fr (O. Hamdaoui)*
[b]*Faculty of Pharmaceutical Engineering Process, Department of Chemical Engineering, University of Constantine 3, 25000 Constantine, Algeria*
[c]*Laboratory of Applied Chemistry and Materials Technology, University of Oum El-Bouaghi, P.O. Box 358, 04000 Oum El-Bouaghi, Algeria, emails: yacinereference@yahoo.com (Y. Rezgui), m_guemini@yahoo.fr (M. Guemini)*

Received 10 February 2014; Accepted 8 July 2014

ABSTRACT

This paper presents a theoretical study of ultrasonic cavitation as an advanced technique for water treatment. A mathematical algorithm, which combines single bubble dynamics model with chemical kinetics mechanism for cavitating bubble, is proposed for estimating the chemical activity of cavitation bubbles. The computer simulations of bubble oscillation and chemical reactions occurring inside a bubble have been performed for various conditions of ultrasonic frequency. The numerical simulations have showed that radicals such as ·OH, H·, and O are created in the bubble during the strong collapse. In all cases, ·OH is the main oxidant created in the bubble. It was found that the generation of the oxidants inside a bubble is strongly frequency dependent. The production rate of the oxidants decreased as the driving ultrasonic frequency increased. It was found that the reaction time is one of the paramount parameters of cavitation that control the extent of radical's generation. Though a direct quantitative comparison between the predicted results in a single bubble and those in bulk solution is impossible, the present theoretical model is able to predict and explain the qualitative trend observed in some experimentally sonochemical phenomena.

Keywords: Ultrasonic cavitation; Bubble dynamics; Chemical Kinetics; Computer simulations; ·OH radicals

1. Introduction

Ultrasonic irradiation of liquids provides a unique environment where high-energy chemical reactions occur at ambient conditions [1]. This has already been used in industrial applications and in the environmental reduction of liquid waste and pollutants [2–6].

The chemical effects of ultrasound arise from acoustic cavitation; that is, ultrasound induced formation, growth and violent collapse of microbubbles in a liquid medium under the rarefaction/compression cycles of the ultrasonic wave (Fig. 1) [7]. The microbubbles formed during the rarefaction part of the ultrasound wave contain vaporized liquid and gas, which was previously dissolved in the liquid. The

*Corresponding author.

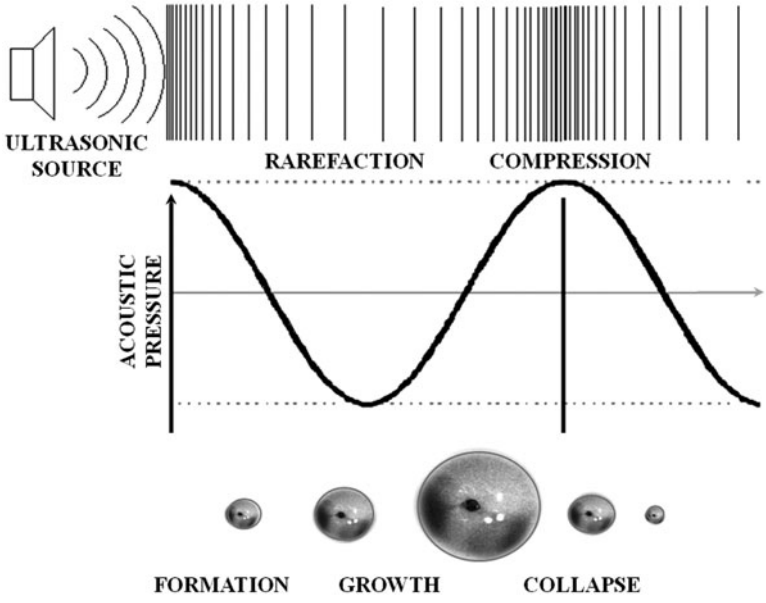

Fig. 1. Dynamics of acoustic cavitation bubble.

lifetime of these microbubbles are of the order of microseconds and their rapid collapse is nearly adiabatic, rendering each individual bubble a microreactor, inside which temperatures of the order of 5,000 K and pressures of hundreds of atmospheres have been shown to exist [8]. As results, water vapor entrapped inside a bubble is thermally dissociated into H· and ·OH radicals, and with other species present, various other reactive species such as $HO_2^{\cdot}$, O, and H_2O_2 may form [9]. A parallel reaction pathway exists where volatile solutes, such as CCl_4 and benzene, may evaporate into the bubble and be pyrolyzed by the high core temperatures [10]. Under certain conditions, bubble collapse can also result in light emission, sonoluminescence (SL), originating from the hot core of the bubble during the final stages of collapse [11]. The radical species produced can recombine, react with other gaseous species present in the cavity, or diffuse out of the bubble into the surrounding liquid to serve as oxidants [10]. Reactions involving free radicals can occur within the collapsing bubble, at the interface of the bubble, and in the surrounding liquid [10]. All chemical reactions promoted by ultrasonic waves are known as sonochemical reactions. Sonochemical oxidation is considered as an emerging advanced oxidation process for water treatment. The efficiency of sonochemical reactions is strongly sensitive to a number of factors, such as applied frequency and spurge gas that control the extent of free radicals generation [12–14].

Several recent studies have attempted to explain the interactions between bubble dynamics and chemical reactions occurring in the bubble. For example, Kamath et al. [15] estimated the production of ·OH radicals at 21 kHz by decoupling the bubble dynamics equation and the chemical kinetics to examine a possible mechanism for the sonoluminescence. Prasad Naidu et al. [16] modeled the equilibrium production of various radicals using the simple Rayleigh–Plesset (RP) equation for the radial motion of the bubble in incompressible liquid coupled with Flynn's assumption that the bubble becomes a closed system during collapse, when the partial pressure of gas becomes equal to the vapor pressure. Gong and Hart [17], Sivasankar et al. [18], and Sochard et al. [19] also adopted a similar approach of coupling bubble dynamic equation with the chemical kinetics consisting on simple reaction mechanism. In the works of Sochard et al. [19] and Sivasankar et al. [18], the mass and heat transfer during bubble oscillation were taken into account. Sivasankar et al. [18] ignored the gas diffusion across the bubble wall as they found that the time scale for the gas diffusion is far higher than the time scale of bubble dynamics. Storey and Szeri [20] showed numerical evidence that the non-equilibrium phase change process has no effects on the maximum bubble temperature when the compression ratio of the bubble is less than 20. The most above-cited works were carried out at low frequencies.

The present paper is part of a research activity concerning theoretical and experimental study of sonochemistry. In this article, a mathematical algorithm (solved in Fortran 90), which combines a model of single bubble dynamics in compressible liquid with chemical kinetics model consisting in complex series of chemical reactions occurring inside an argon bubble, have been used to estimate the chemical activity of the bubble at specified experimental conditions of frequency (the effect of other parameters such as the acoustic amplitude and the liquid temperature on the sonochemical activity of an oxygen bubble have been studied elsewhere [21] at arbitrary conditions). A series of computations of bubble dynamics and chemical reactions inside an argon bubble were performed for various ultrasonic frequencies under the experimental conditions of Ciawi et al. [22]. The obtained results were discussed and used to explain unusual experimentally observed sonochemical phenomena.

2. Model

2.1. Bubble dynamics model

The physical situation of the model is that of a gas- and vapor-filled spherical bubble isolated in water oscillating under the action of a sinusoidal ultrasonic wave. The temperature and pressure in the bubble are assumed to be spatially uniform, and the gas content of the bubble behaves as an ideal gas [23]. The radial dynamics of the bubble is described by a good model furnished by the Keller–Miksis (KM) equation [24–26]:

$$\left(1-\frac{\dot{R}}{c}\right)R\ddot{R}+\frac{3}{2}\left(1-\frac{\dot{R}}{3c}\right)\dot{R}^2 = \frac{1}{\rho_L}\left(1+\frac{\dot{R}}{c}+\frac{R}{c}\frac{\mathrm{d}}{\mathrm{d}t}\right)\left[p-p_\infty-\frac{2\sigma}{R}-4\mu\frac{\dot{R}}{R}+P_A\sin(2\pi ft)\right] \quad (1)$$

in this equation, dots denote time derivatives ($\mathrm{d}/\mathrm{d}t$), R is the radius of the bubble, c is the speed of sound in the liquid, ρ_L is the density of the liquid, σ is the surface tension, μ is the liquid viscosity, p is the pressure inside the bubble, p_∞ is the ambient static pressure, P_A is the acoustic amplitude, and f is the sound frequency. The acoustic amplitude P_A is correlated with the acoustic intensity I_a, or power per unit area, as $P_A = (2I_a\rho_L c)^{1/2}$ [10]. The KM equation (Eq. (1)) is a modification of the RP equation that takes into account the liquid compressibility (the RP equation is obtained when $c\rightarrow\infty$). Due to the rapid progress in the field of high-speed cameras, the confrontation between theory and experiment in the case of large amplitude oscillation highlighted the need to take into account the compressibility. The superimposition of the predicted bubble dynamics curves obtained with RP and KM with the experimental data points showed that the KM equation furnished a good description of the experimental bubble dynamics, whereas the RP curve deviates from the experimental curve, particularly during the bubble collapse [27], which changes greatly the profile of temperature inside a bubble during collapse as can be seen in Ref. [28].

In the present model, the expansion of the bubble is considered as isothermal and its total compression (implosion phase) is treated as adiabatic [29]. These assumptions are widely accepted since the lifetime of an oscillation at high frequency is relatively short with a very rapidly occurring collapse event. We also assume that the vapor pressure in the bubble remains constant during the bubble expansion phase and there is no gas diffusion during expansion and no mass and heat transfer of any kind during collapse. We noticed here that Storey and Szeri [20] demonstrated that the inclusion of non-equilibrium phase change of water vapor at the bubble wall in the bubble dynamics has practically no effect on the maximum bubble temperature attained in the bubble at the collapse when the compression ratio of the bubble (R_{max}/R_{min}) is less than 20. This level of R_{max}/R_{min} was never attained in the present numerical study. Therefore, in order to reduce computational parameters, the current model takes, as input, initial bubble vapor content and neglects mass and heat transfer during bubble expansion and collapse.

Based on the above assumptions, the temperature inside the bubble at any instant during adiabatic phase can be calculated from the bubble size, using the adiabatic law:

$$T = T_\infty\left(\frac{R_{max}}{R}\right)^{3(\gamma-1)} \quad (2)$$

where T_∞ is the bulk liquid temperature, R_{max} is the maximum radius of the bubble, and γ is the ratio of specific heats capacities (c_p/c_v) of the gas/vapor mixture. It is important to notice here that the assumption of spatial uniform pressure and temperature inside the bubble is valid as long as inertia effects are negligible and the velocity of the bubble wall is below the speed of sound in the vapor/gas mixture. This assumption was justified in detail in the paper published by Kamath et al. [15]. In addition, Yasui et al. [30] and Fujikawa and Akamatsu [31] pointed out in

their models which include heat transfer that the bubble temperature and pressure are roughly uniform except at a very thin layer, called thermal boundary, near the bubble wall.

Finally, several physical properties (saturated vapor pressure, density, surface tension, viscosity, and sound velocity) in the above equations change with the liquid temperature T_∞ (water is the liquid medium in this study) and the static pressure p_∞. The equations for the physical properties of water have been described in our previous work [21].

2.2. Chemical kinetics model

Under the experimental condition of Ciawi et al. [22], the bubbles in the cavitating medium are filled with argon and water vapor. For this case, a kinetic mechanism consisting in nineteen reversible elementary chemical reactions (Table 1) is taken into account involving O_2, H_2O, Ar, ·OH, H·, O, $HO_2^{\cdot}$, H_2, and H_2O_2 chemical species. The scheme in Table 1, which has been partially validated from hydrogen flame studies [32] as well as shock-tube and reactor-type experiments [33], includes the most reported chemical reactions inside an argon bubble that have been used by many research groups in sonochemistry and sonoluminescence [15,29,30].

Rate expressions for the chemical reactions consider elementary reversible reactions involving K chemical species, which can be represented in the general form as

$$\sum_{k=1}^{K} \upsilon'_{ki} X_k \leftrightarrow \sum_{k=1}^{K} \upsilon''_{ki} X_k \tag{3}$$

in which υ_{ki} in the stoichiometric coefficients of the ith reaction and X_k is the chemical symbol for the kth species. The superscript ´ indicates forward stoichiometric coefficients, while ´´ indicates reverse stoichiometric coefficients. The production rate $\dot{w}_k$ of the kth species can be written as a summation of the rate of the variables for all reactions involving the kth species:

$$\dot{w}_k = \frac{1}{V}\frac{dn_k}{dt} = \sum_{i=1}^{I} (\upsilon''_{ki} - \upsilon'_{ki}) r_i \quad (k = 1, \ldots, K) \tag{4}$$

where n_k is the number of moles de the kth species and V is the volume of the bubble.

Table 1
The important chemical reactions inside an Ar/H_2O cavitation bubble. M is the third body. Subscript "f" denotes the forward reaction, and "r" denotes the reverse reaction. A is in (cm^3 mol^{-1} s^{-1}) for two-body reaction [(cm^6 mol^{-2} s^{-1}) for a three-body reaction], and E_a is in (cal mol^{-1}).

Reaction	A_f	b_f	E_{af}	A_r	b_r	E_{ar}
R1. H_2O+M ↔ H·+·OH+M	1.912×10^{23}	−1.83	1.185×10^5	2.200×10^{22}	−2.00	0.00
R2. ·OH+M ↔ O+H·+M	9.880×10^{17}	−0.74	1.021×10^5	4.714×10^{18}	−1.00	0.00
R3. O+O+M ↔ O_2+M	6.165×10^{15}	−0.50	0.00	4.515×10^{17}	−0.64	1.189×10^5
R4. H·+O_2 ↔ O+·OH	1.915×10^{14}	0.00	1.644×10^4	5.481×10^{11}	0.39	-2.93×10^2
R5. H·+O_2+M ↔$HO_2^{\cdot}$ +M	1.475×10^{12}	0.60	0.00	3.090×10^{12}	0.53	4.887×10^4
R6. O+H_2O ↔ ·OH+·OH	2.970×10^6	2.02	1.340×10^4	1.465×10^5	2.11	-2.904×10^3
R7. $HO_2^{\cdot}$+H· ↔ H_2+O_2	1.660×10^{13}	0.00	8.230×10^2	3.164×10^{12}	0.35	5.551×10^4
R8. $HO_2^{\cdot}$+H· ↔ ·OH+·OH	7.079×10^{13}	0.00	2.950×10^2	2.027×10^{10}	0.72	3.684×10^4
R9. $HO_2^{\cdot}$+O ↔ ·OH+O_2	3.250×10^{13}	0.00	0.00	3.252×10^{12}	0.33	5.328×10^4
R10. $HO_2^{\cdot}$+·OH ↔ H_2O+O_2	2.890×10^{13}	0.00	-4.970×10^2	5.861×10^{13}	0.24	6.908×10^4
R11. H_2+M ↔ H·+H·+M	4.577×10^{19}	−1.40	1.044×10^5	1.146×10^{20}	−1.68	8.200×10^2
R12. O+H_2 ↔ H·+·OH	3.820×10^{12}	0.00	7.948×10^3	2.667×10^4	2.65	4.880×10^3
R13. ·OH+H_2 ↔ H·+H_2O	2.160×10^8	1.52	3.450×10^3	2.298×10^9	1.40	1.832×10^4
R14. H_2O_2+O_2 ↔ $HO_2^{\cdot}$+$HO_2^{\cdot}$	4.634×10^{16}	−0.35	5.067×10^4	4.200×10^{14}	0.00	1.198×10^4
R15. H_2O_2+M ↔ ·OH+·OH+M	2.951×10^{14}	0.00	4.843×10^4	1.00×10^{14}	−0.37	0.00
R16. H_2O_2+H· ↔ H_2O+·OH	2.410×10^{13}	0.00	3.970×10^3	1.269×10^8	1.31	7.141×10^4
R17. H_2O_2+H· ↔ H_2+$HO_2^{\cdot}$	6.025×10^{13}	0.00	7.950×10^3	1.041×10^{11}	0.70	2.395×10^4
R18. H_2O_2+O ↔ ·OH+$HO_2^{\cdot}$	9.550×10^6	2.00	3.970×10^3	8.660×10^3	2.68	1.856×10^4
R19. H_2O_2+·OH ↔ H_2O+$HO_2^{\cdot}$	1.000×10^{12}	0.00	0.00	1.838×10^{10}	0.59	3.089×10^4

Notes: Third body efficiency factors R1: $\alpha_{H_2} = 0.73$, $\alpha_{H_2O} = 12$, $\alpha_{Ar} = 0.38$, R2: $\alpha_{H_2} = 2.5$, $\alpha_{H_2O} = 12$, $\alpha_{Ar} = 0.83$, R2: $\alpha_{H_2} = 2.5$, $\alpha_{H_2O} = 12$, $\alpha_{Ar} = 0.75$, R5: $\alpha_{H_2} = 1.3$, $\alpha_{H_2O} = 14$, $\alpha_{Ar} = 0.67$, R11: $\alpha_{H_2} = 2.5$, $\alpha_{H_2O} = 12$, R15: $\alpha_{H_2} = 2.5$, $\alpha_{H_2O} = 12$, $\alpha_{Ar} = 0.64$.

The rate r_i for the ith reaction is given by the difference of the forward and reverse rates as

$$r_i = k_{f_i}\prod_{k=1}^{K}[X_k]^{\upsilon'_{ki}} - k_{ri}\prod_{k=1}^{K}[X_k]^{\upsilon''_{ki}} \quad (5)$$

where $[X_k]$ is the molar concentration of the kth species, and k_{fi} and k_{ri} are the forward and reverse rate constants of the ith reaction, respectively. The forward and reverse rate constants for the ith reactions are assumed to have the following Arrhenius temperature dependence:

$$k_{f_i} = A_{f_i}T^{b_{f_i}}\exp\left(-\frac{E_{a_{f_i}}}{R_gT}\right) \quad (6)$$

$$k_{ri} = A_{ri}T^{b_{ri}}\exp\left(-\frac{E_{a_{ri}}}{R_gT}\right) \quad (7)$$

where R_g is the universal gas constant, A_{fi} (A_{ri}) is the pre-exponential factor, b_{fi} (b_{ri}) is the temperature exponent, and E_{fi} (E_{ri}) is the activation energy. Arrhenius parameters of each chemical reaction in Table 1 are obtained from the NIST Chemical Kinetics Database [34].

In some reactions of Table 1, a third body is required for the reaction to process. When a third body is needed, the reaction rate r_i of the ith reaction should be rewritten as:

$$r_i = \left(\sum_{k=1}^{K}\alpha_{ki}[X_k]\right)k_{f_i}\prod_{k=1}^{K}[X_k]^{\upsilon'_{ki}} - k_{ri}\prod_{k=1}^{K}[X_k]^{\upsilon''_{ki}} \quad (8)$$

α_{ki} is the third-body efficiency factor of species k in the ith reaction.

2.3. Procedure of the numerical simulation

The KM equation (Eq. (1)), describing the dynamic of the bubble, is a nonlinear second-order differential equation which requires an approximate numerical method for solution. Eq. (1) can be reduced to a system of two differential first-order equations:

$$\frac{dR}{dt} = \dot{R} \quad (9)$$

$$\frac{d\dot{R}}{dt} = \frac{\frac{1}{\rho_L}\left(1+\frac{\dot{R}}{c}+\frac{R}{c}\frac{d}{dt}\right)\left[p - p_\infty - \frac{2\sigma}{R} - 4\mu\frac{\dot{R}}{R} + P_A\sin(2\pi ft)\right] - \frac{3}{2}\left(1-\frac{\dot{R}}{3c}\right)\dot{R}^2}{\left(1-\frac{\dot{R}}{c}\right)R} \quad (10)$$

As the expansion of the bubble is isothermal and the subsequent collapse is adiabatic, the pressure inside a bubble (p) is expressed as

- Expansion phase ($R_0 \le R \le R_{max}$ and $dR/dt0$) :

$$p = P_v + P_{g0}\left(\frac{R_0}{R}\right)^3 \quad (11)$$

- Collapse phase ($R_{min} \le R \le R_{max}$ and $dR/dt \le 0$) :

$$p = \left[P_v + P_{g0}\left(\frac{R_0}{R_{max}}\right)^3\right]\left(\frac{R_{max}}{R}\right)^{3\gamma} \quad (12)$$

where P_v is the saturated vapor pressure, $P_{g0} = p_\infty + (2\sigma/R_0) - P_v$ is the gas pressure in the bubble at its ambient state ($R = R_0$). The transition from isothermal expansion to adiabatic collapse occurs when the bubble wall velocity dR/dt changes the sign from positive to negative at around the maximum bubble radius (R_{max}).

The system of Eqs. (9) and (10) was solved by the fourth-order Runge–Kutta method with a fixed step (2×10^{-4} μs) using the following initial conditions:

at $t = 0$, $R = R_0$, and $\dot{R} = 0$

The physical properties in the above equations are estimated for water at 20°C as [21] ρ_L = 998.12 kg m^{-3}, σ = 72.45 × 10^{-3} N m^{-1}, μ = 10^{-3} kg s^{-1} m^{-1}, and c = 1,482 m s^{-1}.

The simulation of the chemical reactions in the bubble starts at the beginning of the adiabatic phase (at time corresponding to $R = R_{max}$). The application of Eq. (4) for all species (9 species) involved in the scheme of Table 1 gives a system of nine ordinary differential equations. For example, according to Table 1, the application of Eq. (4) to the H_2O species gives:

$$\begin{aligned} w_k = \frac{1}{V}\frac{dn_{H_2O}}{dt} &= -\left\{k_{f1}[H_2O][M] - k_{r1}[H^\cdot][^\cdot OH][M]\right\} \\ &\quad - \left\{k_{f3}[H_2O][O] - k_{r3}[^\cdot OH]^2\right\} \\ &\quad - \left\{k_{f6}[H_2O][H] - k_{r6}[H_2][^\cdot OH]\right\} \\ &\quad - \left\{k_{f9}[H_2O][HO_2^\cdot] - k_{r9}[H_2O_2][^\cdot OH]\right\} \end{aligned} \quad (13)$$

where V is the volume of the bubble and n_{H_2O} is the number of moles of H_2O.

Using the ideal gas law $PV = n_tRT$, Eq. (13) can be rewritten as

$$\frac{dn_{H_2O}}{dt} = -\frac{ntRT}{p} \times \left\langle \begin{array}{l} \{k_{f1}[H_2O][M] - k_{r1}[H^{\cdot}][^{\cdot}OH][M]\} + \{k_{f3}[H_2O][O] - k_{r3}[^{\cdot}OH]^2\} - \\ \{k_{f6}[H_2O][H] - k_{r6}[H_2][^{\cdot}OH]\} + \{k_{f9}[H_2O][HO_2^{\cdot}] - k_{r9}[H_2O_2][^{\cdot}OH]\} \end{array} \right\rangle \quad (14)$$

where n_t is number of mole of all species present in the bubble.

The input parameters for solving the system of the ordinary differential equations obtained by Eq. (4) are the composition of the bubble on water vapor and argon at time corresponding to $R = R_{max}$, the temperature and pressure profiles in the bubble during adiabatic phase and the collapse time. These parameters are obtained by solving the dynamic equation (Eq. (1)). As the bubble temperature increases during the adiabatic phase, the reaction system evolves and radicals start to form by thermal dissociation of H_2O in the bubble. Thus, the composition of the bubble on all species expected to be present was determined at any temperature during the collapse period by solving the system of the ordinary differential equations obtained by Eq. (4). The system of the ordinary differential equations was solved by the finite difference method. The computer simulation of the reactions system was stopped after the end of the bubble collapse.

3. Results and discussion

In this study, numerical simulations of the bubble oscillations are performed under the experimental conditions of Ciawi et al. [22]. Ciawi et al. [22] have measured the bubble temperatures in aqueous *tert*-butyl alcohol solutions using a methyl radical recombination method at three ultrasound frequencies (20, 355, and 1,056 kHz). The solutions were saturated with argon prior to sonication, and the acoustic power was 28 W. By extrapolating the temperatures measured to zero concentration of *tert*-butyl alcohol, at bulk solution temperature of 20 °C, the bubble temperatures in liquid water were estimated to be 3,400 K at 20 kHz, 4,300 K at 355 kHz, and 3,700 K at 1,056 kHz.

Because most of the important researches on sonochemistry are performed at ultrasonic frequencies in the range of 200–1,000 kHz, the numerical simulations of this study have been performed at only 355 and 1,056 kHz.

One of the important parameters for the numerical simulations of the bubble oscillations is the ambient bubble radius, R_0, which is defined as the bubble radius when ultrasound is absent. The ambient bubble radii were determined as 5.9 μm and 1.5 μm for, respectively, 355 and 1,056 kHz to reproduce the experimentally maximum bubble temperatures of 4,300 K and 3,700 K for, respectively, 355 and 1,056 kHz, under the experimental conditions of Ciawi et al. [22]. These determined values of R_0 with respect to frequency are in good agreement with those furnished by the experiments for nearly the same conditions of ultrasound frequencies (Labouret and Frohly [35] determined a mean ambient bubble radius in the range of 5–7 μm at 350 kHz using an electromagnetic method, and Chen et al. [36] and Brotchie et al. [37] determined a mean ambient radii of 1.4 μm and 2 μm at 1,100 kHz, and 1,056 kHz, respectively, using detected active cavitation and pulsed ultrasound methods). Thus, the ambient bubble size is the first parameter that is strongly influenced by the ultrasonic frequency in ultrasonic cavitational field.

In Fig. 2(a) and (b) the calculated results of the R/R_0 ratio and the temperature inside a bubble have been shown as function of time for the two ultrasonic frequencies. In all cases, the bubble initially expands, passes through a maximum (more than two times of the ambient bubble radius) and then quickly collapses at less than 6% of its initial radius during the final stage of the collapse. The same behavior of the bubble radius history was detected experimentally as reported by several research studies [38–40]. The end of the bubble collapse is indicated by black dotes in Fig. 2(a) and (b). On the other hand, the temperature inside a bubble remains constant during the expansion phase and the first stage of the collapse phase and then sharply increases during the final stage of the bubble collapse up to 4,300 K and 3,700 K for, respectively, 355 and 1,056 kHz, which are the temperatures determined experimentally by Ciawi et al. [22]. The same behavior was observed for the pressure inside a bubble that attained maximum values of 150 atm and 118 atm for, respectively, 355 kHz and 1,056 kHz. The existence of such extreme conditions of temperatures and pressures inside a bubble provides a unique means for driving chemical reactions.

In Fig. 3(a) and (b), the simulations results of the chemical reactions evolution inside a bubble are shown as function of time at around the end of the bubble collapse for the two ultrasonic frequencies. The profiles of temperatures inside a bubble are also inserted in these Figures. The principal vertical axes in Fig. 3(a) and (b) are in logarithmic scale. For a bubble initially composed of argon and water vapor, when the bubble temperature and pressure inside a bubble increases drastically during the strong collapse, a large amount of the trapped water vapor is dissociated and many chemical products such as H_2, O_2, $^{\cdot}OH$, $H^{\cdot}$, O, $HO_2^{\cdot}$ and H_2O_2, are created (Fig. 3). The $HO_2^{\cdot}$ and H_2O_2 were not found to be formed at appreciable

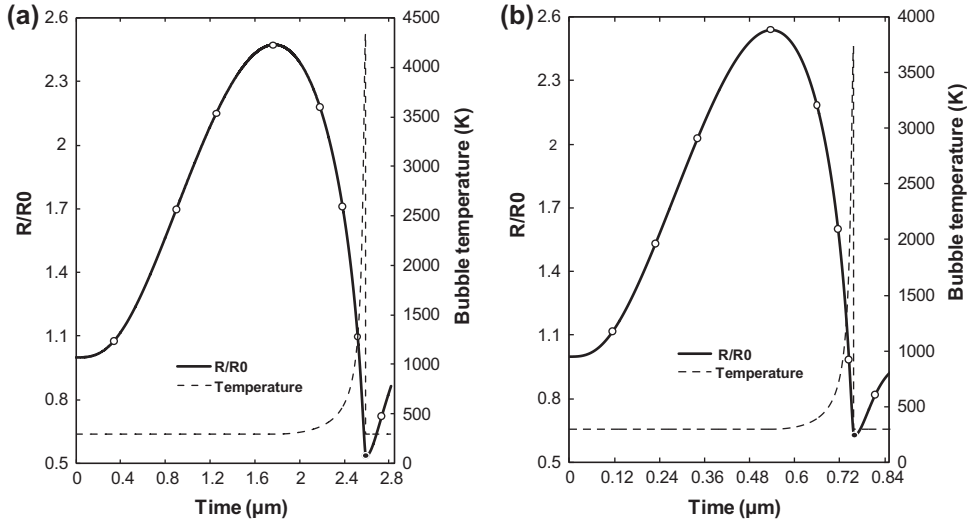

Fig. 2. R/R_0 ratios and bubbles temperatures as function of time for (a) 355 kHz and (b) 1,056 kHz (conditions: ambient bubble radii: 5.9 μm for 355 μm and 1.5 μm for 1,056 kHz; acoustic power: 28 W; liquid temperature: 20˚C; static pressure: 1 atm). The maximum bubble radii are 14.6 μm and 3.81 μm for, respectively, 355 and 1,056 kHz. The bubble lifetimes are 2.6 μs and 0.757 μs for, respectively, 355 and 1,056 kHz. The bubble collapse times are 0.85 μs and 0.253 μs for, respectively, 355 and 1,056 kHz.

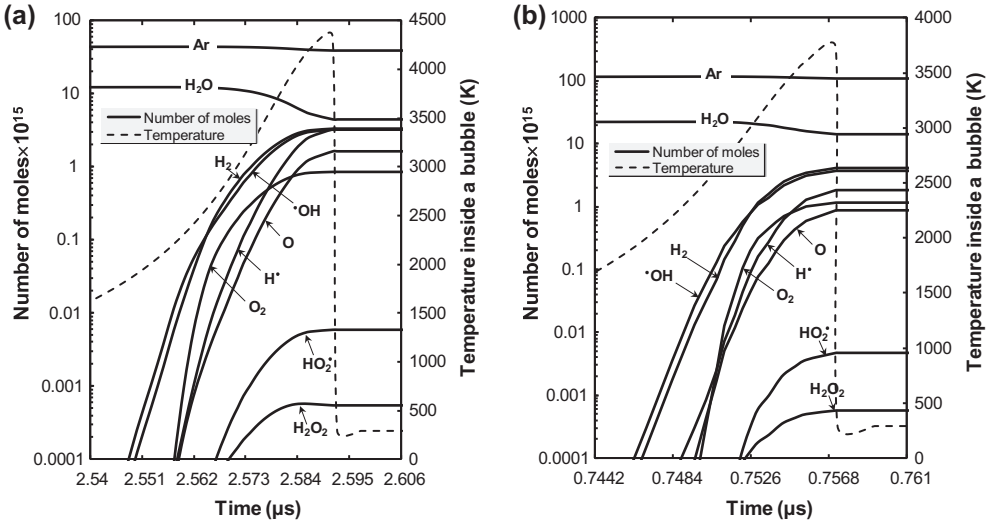

Fig. 3. Enlarged views of the chemical reactions evolution inside a bubble as function of time at around the end of the bubble collapse for (a) 355 kHz and (b) 1,056 kHz. The principal vertical axes (number of moles) are in logarithmic scale (conditions: ambient bubble radii: 5.9 μm for 355 μm and 1.5 μm for 1,056 kHz; acoustic power: 28 W; temperature: 20˚C; static pressure: 1 atm). The horizontal axes are only for 0.066 μs in (a) and 0.0168 μs in (b).

amount in an argon bubble. The mean reactions responsible for the production of the main chemical oxidants (•OH, H•, and O) formed are determined from the chemical kinetics analysis and are presented in Table 2. It should be noted here that under the sonication conditions of Ciawi et al. [22], the numerical simulations have indicated that cavitation bubbles are nearly gaseous because more than 80% of the trapped argon is remained in the bubble at the end of the bubble collapse. From Fig. 3(a) and (b), it is clearly seen that the reaction time, which is the difference between the time of the end of the first bubble collapse and the time at which the reaction products start to form, decreases as the ultrasonic frequency increases

Table 2
The main reactions (and their contribution in the production) responsible for the production of the main oxidants (·OH, H·, and O) formed inside an argon bubble at the end of the bubble collapse. Results obtained from the chemical kinetics analysis

Species	355 kHz	1,056 kHz
·OH	$H_2O + M \rightarrow H^{\cdot} + {}^{\cdot}OH + M$ (~58%)	$H_2O + M \rightarrow H^{\cdot} + {}^{\cdot}OH + M$ (~58%)
	$H^{\cdot} + H_2O \rightarrow {}^{\cdot}OH + H_2$ (~22%)	$H^{\cdot} + H_2O \rightarrow {}^{\cdot}OH + H_2$ (~39%)
H·	$H_2O + M \rightarrow H^{\cdot} + {}^{\cdot}OH + M$ (~59%)	$H_2O + M \rightarrow H^{\cdot} + {}^{\cdot}OH + M$ (~67%)
	$^{\cdot}OH + M \rightarrow O + H^{\cdot} + M$ (17%)	$O + {}^{\cdot}OH \rightarrow H^{\cdot} + O_2$ (~19%)
O	$H^{\cdot} + {}^{\cdot}OH \rightarrow O + H_2$ (~58%)	$H^{\cdot} + {}^{\cdot}OH \rightarrow O + H_2$ (~73%)
	$^{\cdot}OH + M \rightarrow O + H^{\cdot} + M$ (~41%)	$^{\cdot}OH + M \rightarrow O + H^{\cdot} + M$ (~22%)

(0.04 μs at 355 kHz and 0.011 μs at 1,056 kHz). It is also seen that the main molecular product for an argon bubble is H_2 for all frequencies, whereas the main oxidants are ·OH and H· radicals and O atoms. The amount of each chemical product created inside a bubble reached their upper limit (critical value) at the end of the bubble collapse as the temperature and pressure attained their upper values at this point. The production of each oxidant remained constant after the end of the bubble collapse, showing a similar trend as that reported by Yasui et al. [41] using a more detailed model that includes the effect of thermal condition and non-equilibrium phase change. It was also seen from Figs. 2 and 3 that the bubble temperature suddenly drops to the ambient temperature just after the minimum bubble radius. This behavior, which results from the assumption of the adiabatic collapse and isothermal expansion, differs slightly from that of a real bubble as can be seen in Ref. [30]. However, this will not affect the calculated chemical bubble yield at the end of the bubble collapse (at R_{min}), for which are based the calculations of Tables 2 and 3. For verifying the effect of non-equilibrium condensation and evaporation of water vapor at the bubble wall, a simple quantitative comparison between our model and Yasui's model [42] that includes the neglected parameters has been carried elsewhere [43] on the basis of the range of ambient radius for the production of the oxidants. At 1,000 kHz [42], Yasui et al. reported a range of 0.1–3 μm. For the same conditions, we have calculated a range of ~0.3–3.8 μm [44] with our model that neglects mass and heat transfer during oscillation. The conclusion was that our results agree with the results of Yasui et al. [42] and the slightly observed difference is due to the different nature of bubbles: sonoluminescing bubble (SL) in Yasui's study and sonochemically active bubble in our study (the range of ambient radius for SL bubble is smaller than that of sonochemically active bubble [45]). This simple comparison showed that the range of ambient bubble radius for the production of the oxidants is the same with and without including non-equilibrium phase change of water vapor at the bubble wall, which supports the results of Storey and Szeri [20] concerning the nonsignificance of the non-equilibrium phase change of water vapor and also the chemistry inside a bubble on the maximum bubble temperature when the bubble compression ratio (R_{max}/R_{min}) is less than 20.

Table 3
Production rate of the main chemical oxidants (·OH, H·, and O) created inside an argon bubble as function of frequency

	Rate of production (mol s^{-1})	
Species	355 kHz	1,056 kHz
·OH	1.15×10^{-9}	3.88×10^{-11}
H·	1.15×10^{-9}	1.94×10^{-11}
O	5.83×10^{-10}	9.32×10^{-12}

Now, in order to carry out a comparison for the same time of oscillation, let us use the rate of production for each species, which is defined as the amount of the species inside a bubble after it becomes nearly constant after the first bubble collapse multiplied by ultrasonic frequency [45]. The obtained results in term of rate of production are presented in Table 3. According to this table, the production rate of each of the oxidants created in the bubble decreases as the frequency increases. It should be noted here that this result is, qualitatively, in good agreement with that reported in aqueous solution, which suggest a lower sonochemical activity at very high frequency. For example, Pétrier and co-workers examined the sonochemical production of H_2O_2 and degradation of phenol [4], bisphenol A [13], and chlorophenols [46] at various frequencies in the range of 200–800 kHz. They found that the

efficiency of sonochemical reaction (production of H_2O_2 and degradation of pollutants) decreases as the frequency of ultrasound increases. Kanthale et al. [47] found that both sonochemistry (H_2O_2 yield) and sonoluminescence intensity decreases with increasing frequency in the range 213–1,056 kHz. Beckett and Hua [12] showed that rates of H_2O_2 production, 1,4-dioxane decomposition, and luminescence intensity decrease as the ultrasonic frequency increases in the interval 358–1,071 kHz.

It should be noted that the overall sonochemical activity in aqueous solution is not related only to the single bubble event, but also to the number of bubbles formed in the cavitating medium, which are in turn strongly affected by the ultrasonic frequency. As a result, the application of the model to a particular solute or pollutant needs the knowledge of the number of collapsing bubbles in the cavitating mediums where the literature in this field is very scarce, practically due to the complicated nature of the phenomena. Without exact information about the number of bubbles, the application of any single bubble model to a particular solute is impossible. Given all these considerations, it clearly appears that the predicted trends of the sonochemical yields in single bubble are consistent with that in bulk solutions observed in various reports on the effect of ultrasonic frequency on the sonochemistry reaction yield.

Finally, this study clearly showed that the extent of radical's formation in single cavitation bubble is not only function of the peak temperature and pressure reached in the bubble during the transient collapse and the amount of water vapor entrapped in the bubble at the collapse. The other parameter of paramount importance is the reaction time that is strongly sensitive to the variation in operational conditions, such as ultrasonic frequency. This conclusion supports the hypothesis of Ashokkumar and Grieser [48] that showed that the temperature responsible for the chemical reactions is a time and volume average temperature.

4. Conclusions

In the present paper, a theoretical model that combines a dynamic of single cavitation bubble with the chemical kinetics inside an argon bubble has been used for studding ultrasonic cavitation as an advanced technique for water treatment. The numerical simulations showed that the strong collapse of acoustic bubbles generates ·OH radicals as a dominant oxidizing species. It is shown that the generation of the free radicals inside a bubble is a strongly depended on frequency of the sound wave. The amount of radicals created in the bubble was found to be decreased when the ultrasonic frequency increased. The results of this study showed that the third parameter of the paramount importance for the generation of radicals in single bubble is the reaction time. The model presented in this paper was suitable for predicting the trend of the ultrasonic frequency influence on sonochemical reactions.

Acknowledgements

The financial support by the Ministry of Higher Education and Scientific Research of Algeria (project No. J0101120120098) is greatly acknowledged.

Nomenclature

c	—	speed of sound in the liquid medium (m s^{-1})
f	—	frequency of ultrasonic wave (Hz)
I_a	—	acoustic intensity of ultrasonic irradiation (W m^{-2})
n_k	—	number of moles de the kth species (mol)
p	—	pressure inside a bubble (Pa)
p_∞	—	ambient static pressure (Pa)
P_A	—	amplitude of the acoustic pressure (Pa)
P_v	—	vapor pressure of water (Pa)
P_{g0}	—	initial gas pressure (Pa)
R	—	radius of the bubble (m)
R_{max}	—	maximum radius of the bubble (m)
R_0	—	ambient bubble radius (m)
t	—	time (s)
T	—	temperature inside a bubble (K)
T_∞	—	ambient liquid temperature (K)
V	—	volume of the bubble (m^3)

Greek letters

γ	—	specific heat ratio (c_p/c_v) of the gas mixture
σ	—	surface tension of liquid water (N m^{-1})
ρ	—	density of liquid water (kg m^{-3})
μ	—	viscosity of liquid water (N m^{-2} s)

References

[1] T.G. Leighton, The Acoustic Bubble, Academic Press, London, 1994.
[2] A. Gedanken, Using sonochemistry for the fabrication of nanomaterials, Ultrason. Sonochem. 11 (2004) 47–55.
[3] T.J. Mason, L. Paniwnyk, J.P. Lorimer, The uses of ultrasound in food technology, Ultrason. Sonochem. 3 (1996) S253–S260.
[4] C. Pétrier, A. Francony, Ultrasonic waste-water treatment: Incidence of ultrasonic frequency on the rate of phenol and carbon tetrachloride degradation, Ultrason. Sonochem. 4 (1997) 295–300.
[5] M.R. Hoffmann, I. Hua, R. Höchemer, Application of ultrasonic irradiation for the degradation of chemical contaminants in water, Ultrason. Sonochem. 3 (1996) S163–S172.

[6] J. Park, N. Her, Y. Yoon, Ultrasonic degradation of bisphenol A, 17β-estradiol, and 17α-ethinyl, Desalin. Water Treat. 30 (2011) 300–309.
[7] K.S. Suslick, Y. Didenko, M.M. Fang, T. Hyeon, K.J. Kolbeck, W.B. McNamara, M.M. Mdleleni, M.M. Wong, Acoustic cavitation and its chemical consequences, Philos. Trans. R. Soc. A: Math. Phys. Eng. Sci. 357 (1999) 335–353.
[8] L.H. Thompson, L.K. Doraiswamy, Sonochemistry: Science and engineering, Ind. Eng. Chem. Res. 38 (1999) 1215–1249.
[9] P. Riesz, D. Berdahl, C.L. Christman, Free radical generation by ultrasound in aqueous and nonaqueous solutions, Environ. Health Perspect. 64 (1985) 233–252.
[10] Y.G. Adewuyi, Sonochemistry: Environmental science and engineering applications, Ind. Eng. Chem. Res. 40 (2001) 4681–4715.
[11] K.S. Suslick, D.J. Flannigan, Inside a collapsing bubble: Sonoluminescence and the conditions during cavitation, Annu. Rev. Phys. Chem. 59 (2008) 659–683.
[12] M.A. Beckett, I. Hua, Impact of ultrasonic frequency on aqueous sonoluminescence and sonochemistry, J. Phys. Chem. A 105 (2001) 3796–3802.
[13] R.A. Torres, C. Pétrier, E. Combet, M. Carrier, C. Pulgarin, Ultrasonic cavitation applied to the treatment of bisphenol A. Effect of sonochemical parameters and analysis of BPA by-products, Ultrason. Sonochem. 15 (2008) 605–611.
[14] E.L. Mead, R.G. Sutherland, R.E. Verrall, The effect of ultrasound on water in the presence of dissolved gases, Can. J. Chem. 54 (1976) 1114–1120.
[15] V. Kamath, A. Prosperetti, F.N. Egolfopoulos, A theoretical study of sonoluminescence, J. Acoust. Soc. Am. 94 (1993) 248–260.
[16] D.V. Prasad Naidu, R. Rajan, R. Kumar, K.S. Gandhi, V.H. Arakeri, S. Chandrasekaran, Modelling of a batch sonochemical reactor, Chem. Eng. Sci. 49 (1994) 877–888.
[17] C. Gong, D.P. Hart, Ultrasound induced cavitation and sonochemical yields, J. Acoust. Soc. Am. 104 (1998) 2675–2682.
[18] T. Sivasankar, A.W. Paunikar, V.S. Moholkar, Mechanistic approach to enhancement of the yield of a sonochemical reaction, AIChE J. 53 (2007) 1132–1143.
[19] S. Sochard, A.M. Wilhelm, H. Delmas, Modelling of free radicals production in a collapsing gas-vapour bubble, Ultrason. Sonochem. 4 (1997) 77–84.
[20] B.D. Storey, A.J. Szeri, Water vapour, sonoluminescence and sonochemistry, Proc. R. Soc. A: Math., Phys. Eng. Sci. 456 (2000) 1685–1709.
[21] S. Merouani, O. Hamdaoui, Y. Rezgui, M. Guemini, Computer simulation of chemical reactions occurring in collapsing acoustical bubble: Dependence of free radicals production on operational conditions, Res. Chem. Intermed. In press (2013), doi: 10.1007/s11164-013-1240-y.
[22] E. Ciawi, J. Rae, M. Ashokkumar, F. Grieser, Determination of temperatures within acoustically generated bubbles in aqueous solutions at different ultrasound frequencies, J. Phys. Chem. B 110 (2006) 13656–13660.
[23] L.A. Crum, The polytropic exponent of gas contained within air bubbles pulsating in a liquid, J. Acoust. Soc. Am. 73 (1983) 116–120.
[24] J.B. Keller, M.J. Miksis, Bubble oscillations of large amplitude, J. Acoust. Soc. Am. 68 (1980) 628–633.
[25] V. Kamath, A. Prosperetti, Numerical integration methods in gas-bubble dynamics, J. Acoust. Soc. Am. 85 (1989) 1538–1548.
[26] A. Prosperetti, The equation of bubble dynamics in a compressible liquid, Phys. Fluids 30 (1987) 3626–3628.
[27] F.R. Young, Sonoluminescence, CRC Press, Boca Raton, FL, 2005.
[28] D. Fuster, C. Dopaza, G. Hauke, Liquid compressibility effects during the collapse of a single cavitating bubble, J. Acoust. Soc. Am. 129 (2011) 122–133.
[29] A.J. Colussi, L.K. Weavers, M.R. Hoffmann, Chemical bubble dynamics and quantitative sonochemistry, J. Phys. Chem. A 102 (1998) 6927–6934.
[30] K. Yasui, T. Tuziuti, M. Sivakumar, Y. Iida, Theoretical study of single-bubble sonochemistry, J. Chem. Phys. 122 (2005) 224706.
[31] S. Fujikawa, T. Akamatsu, Effects of the non-equilibrium condensation of vapour on the pressure wave produced by the collapse of a bubble in a liquid, J. Fluid Mech. 97 (1980) 481–512.
[32] M.O. Conaire, H.J. Curran, J.M. Simmie, W.J. Pitz, C.K. Westbrook, A comprehensive modeling study of hydrogen oxidation, Int. J. Chem. Kinet. 36 (2004) 603–622.
[33] M.A. Mueller, T.J. Kim, R.A. Yetter, F.L. Dryer, Flow reactor studies and kinetic modeling of the H_2/O_2 reaction, Int. J. Chem. Kinet. 31 (1999) 113–125.
[34] NIST Chemical Kinetics Database. Available from: http://kinetics.nist.gov/index.php.
[35] S.Labouret, J.Frohly, Distribution en tailles des bulles d'un champ de cavitation ultrasonore (Bubble size distribution in a field of ultrasonic cavitation), 10ème Congrès Français d'Acoustique, April, 12–16, Lyon, 2010.
[36] W.-S. Chen, T.J. Matula, L.A. Crum, The disappearance of ultrasound contrast bubbles, Ultrasound Med. Biol. 28 (2002) 793–803.
[37] A. Brotchie, F. Grieser, M. Ashokkumar, Effect of power and frequency on bubble-size distributions in acoustic cavitation, Phys. Rev. Lett. 102 (2009) 084302-1–084302-4.
[38] S.J. Putterman, K.R. Weninger, Sonoluminescence: How bubbles turn sound into light, Annu. Rev. Fluid Mech. 32 (2000) 445–476.
[39] B.P. Barber, C.C. Wu, R. Lofsted, P.H. Roberts, S.J. Putterman, Sensitivity of sonoluminescence to experimental parameters, Phys. Rev. Lett. 72 (1994) 1380–1383.
[40] T.J. Matula, Inertial cavitation and single-bubble sonoluminescence, Philos. Trans. R. Soc. A: Math., Phys. Eng. Sci. 357 (1999) 225–249.
[41] K. Yasui, T. Tuziuti, Y. Iida, H. Mitome, Theoretical study of the ambient-pressure dependence of sonochemical reactions, J. Chem. Phys. 119 (2003) 346–356.
[42] K. Yasui, Influence of ultrasonic frequency on multibubble sonoluminescence, J. Acoust. Soc. Am. 112 (2002) 1405–1413.
[43] S. Merouani, O. Hamdaoui, Y. Rezgui, M. Guemini, Theoretical procedure for the characterization of

acoustic cavitation bubbles, Acta Acust. United Acust. (2014), accepted manuscript.
[44] S. Merouani, O. Hamdaoui, Y. Rezgui, M. Guemini, Effects of ultrasound frequency and acoustic amplitude on the size of sonochemically active bubbles—Theoretical study, Ultrason. Sonochem. 20 (2013) 815–819.
[45] K. Yasui, T. Tuziuti, J. Lee, T. Kozuka, A. Towada, The range of ambient radius for an active bubble in sonoluminescence and sonochemical reactions, J. Chem. Phys. 128 (2008) 184705-1–184705-12.
[46] C. Pétrier, D. Casadonte, The sonochemical degradation of aromatic and chloroaromatic contaminants, Adv. Sonochem. 6 (2001) 91–109.
[47] P. Kanthale, F. Ashokkumar, F. Grieser, Sonoluminescence, sonochemistry (H_2O_2 yield) and bubble dynamics: Frequency and power effects, Ultrason. Sonochem. 15 (2008) 143–150.
[48] M. Ashokkumar, F. Grieser, A comparison between multibubble sonoluminescence intensity and the temperature within cavitation bubbles, J. Am. Chem. Soc. (2005) 5326–5327.